Int. J. Electrochem. Sci., 10 **(2015)** 10402 - 10421

International Journal of
ELECTROCHEMICAL
SCIENCE
www.electrochemsci.org

Monitoring Marine Atmospheric Corrosion by Electrochemical Impedance Spectroscopy under Various Relative Humidities

Xiumin Ma[1,*], *Qingli Cheng*[1], *Meng Zheng*[1], *Fangying Cui*[1,2], *Baorong Hou*[1]

[1] Institute of Oceanology, Chinese Academy of Sciences, 7 Nanhai Road, Qingdao 266071, PR China
[2] Chongqing University, 174 Shazheng Road, Chongqing 400044, PR China
[*]E-mail: xma@qdio.ac.cn

Received: 16 April 2015 / *Accepted:* 20 September 2015 / *Published:* 4 November 2015

Multielectrode sensors based on electrochemical impedance spectroscopy (EIS) were developed for monitoring marine atmospheric corrosion in simulated marine environment with various relative humidities and fixed chloride ion content. The results show that at 40–60% RH, EIS results reflect the electrode characters, whereas at 75–100% RH, it is proved that EIS measurements can be used to monitor the atmospheric corrosion rate. The reciprocal of the charge transfer resistance provided quantitative change trend of corrosion rate and showed a similar change trend with the reciprocal of the polarization resistance, which was verified by weight loss.

Keywords: B. EIS; B. Weight loss; C. Atmospheric corrosion.

1. INTRODUCTION

The corrosion of metallic structures could cause significant damage to the infrastructure, transportation, utilities, production, and manufacturing industries, in atmospheric environments, particularly in the coastal regions, where the contribution of airborne salinity to structural degradation is greater than that of industrial pollutants [1]. Deposition of airborne salts is one of the main reasons for the reduction of the service life of metal components. Therefore, the detection of marine atmospheric corrosion is of great practical importance.

Traditionally, atmospheric corrosion is qualitatively assessed by observation after a time exposure to an accelerated aging environment. Several conventional methods, such as Raman spectroscopy [2], X-ray diffraction [3,4], scanning electron microscopy (SEM) [3,5], environmental SEM [6], X-ray photoelectron spectroscopy [7] and atomic force microscopy [8], have been extensively used to evaluate atmospheric corrosion. However, these methods cannot provide continuous and in situ information on the atmospheric corrosion process. Although gravimetric methods [9,10] are highly reliable, these techniques require removal of corrosion products by chemical

or mechanical treatment, which is time-consuming, and could not provide in situ information either. As a result, the development of alternative testing methods that are sufficiently fast for in situ monitoring of atmospheric corrosion is vital**.**

Atmospheric corrosion is primarily an electrochemical process. As a result, the instantaneous monitoring of atmospheric corrosion based on electrochemical measurements has attracted the interest of many researchers [11–20]. Moreover, atmospheric corrosion monitors (ACMs) have been used to detect electrochemical signals. However, these methods have their limitations. The scanning Kelvin probe (SKP) [11,21,22], which is used to investigate corrosion under thin electrolyte layers (TELs), causes strong convective effects on sample TEL surfaces because of SKP oscillations during measurements [23]. Therefore, it is very hard to get accurate information on the corrosion process. Although giant magnetoresistive sensors [18] are low-cost, their principal drawback is their relatively low sensitivity and inability to distinguish between corrosion processes that vary in cell lengths because of the varying material/environment combinations. Meanwhile, the major limitation of electrical resistance (ER) sensors is the lengthy response time and the difficulty of measuring the corrosion rate in the initial stage of corrosion or in relatively mild corrosive environments [24]. The low reliability of ER increases when severe pitting corrosion occurs without any significant metal loss and resistance change in the sensor [25]. Screen-printed ACM [14] provides data on the corrosion severity and does not provide direct information on the prevailing electrochemical processes and then can lead to open circuits during long-term monitoring. Meanwhile, coupled multielectrode array sensor (CMAS) probes have been used to measure the nonuniform corrosion rates of carbon steel and stainless steel under salt deposits in air [26,27] and in saturated aqueous solutions [28]. However, CMAS systems also have limitations depending on their operating principles. A noticeable limitation of the CMAS probe is the underestimation of actual dissolution rates because of the concurrent cathodic reactions occurring on the most anodic electrode of the array. The electrochemical monitoring of outdoor corrosion has been conducted through the measurement of a galvanic couple, which can be readily analysed [29,30]. However, the quantitative information on the corrosion rate itself cannot be derived from the galvanic current. The greatest difficulty in the application of this technique is that the solution resistance becomes extremely high under TELs. In such conditions, an extremely high ohmic drop can produce errors in the atmospheric corrosion rate.

Electrochemical impedance spectroscopy (EIS) is a vital technique for the investigation of the atmospheric corrosion of metals under TELs [13,31]. The solution resistance can be estimated from the impedance measured at the high-frequency (HF) region, whereas the sum of the polarisation and solution resistances can be estimated from the low-frequency (LF) region. EIS provides a non-destructive assessment of the atmospheric corrosion behaviour and can also be utilised to study corrosion mechanisms. The electrode surface conditions do not change during EIS measurement because of the use of low-amplitude perturbation. Therefore, EIS can be applied in the in situ monitoring of corrosion. Meanwhile, the current passing through the working electrode (WE) and counter electrode (CE) is extremely small because of the low disturbance amplitude. This phenomenon suggests that the effect of solution resistance on electrochemical measurements under TELs is negligible. Nishikata et al. [12] used EIS to investigate the atmospheric corrosion of 304 stainless steel (304SS) covered with a 10 μm to1000 μm thick NaCl solution layer. Yadav et al. [32] used EIS to

monitor the atmospheric corrosion of zinc under wet and dry cyclic conditions in laboratory. Dubuisson et al. [31] conducted EIS to analyse galvanised steel under an electrolyte droplet in an atmospheric environment. An EIS-based, two-electrode system with comb-like arrangement was successfully applied to monitor atmospheric corrosion [16,19]. Although the quantified parameters for monitoring the corrosion process using EIS remain to be discussed, the results showed that the current distribution on the comb-like electrode surface was uneven [16]. Nevertheless, obtaining more accurate information on the corrosion process is vital in achieving uniform current distribution.

The TEL thickness and the current distribution on the electrode surface can be controlled by introducing a reference electrode (RE) to measure the potential of the electrode during atmospheric corrosion, which causes errors in electrochemical measurements. The CE can then be utilised as an RE in a two-electrode system. Thus, in this study, a two-electrode system with a multielectrode arrangement was used to monitor the marine atmospheric corrosion of zinc under different relative humidities (RHs) in laboratory-simulated environments. Nyrkova et. al [20] have reported on multielectrode sensors with cosurface arrangement of electrodes. However, the sensors cannot be used in remote regions and thus lead to the introduction of errors during determination of the corrosion rate.

Based on the aforementioned analysis, one advantage of Multielectrode sensors (MSs) is that it could overcome the limitations of the previously discussed atmospheric corrosion sensors. In MS, the actual dissolution rates would not be underestimated because the WEs and the CEs are integrated, respectively, the errors caused by extremely high ohmic drops will not occur, and open circuits would be prevented during long-term monitoring. In addition, the initial corrosion rate, corrosion severity, and electrochemical processes can be observed by EIS. Another advantage of MSs is that it can be used to measure multiple locations and thus increase the success rate of EIS measurements under thin and possibly noncontinuous water layers under atmospheric conditions. Thus, the single two-electrode system was replaced by MSs.

This study aims to prove that EIS measurements using MSs can be successfully used to investigate atmospheric corrosion in actual marine field environments, yield reliable EIS data, and identify the required parameters. The system can also be used as a wire beam electrode, which can be utilised to measure potential [33] and detect the nonuniform corrosion thermodynamics and kinetics over electrode surfaces [34,35]. Ultimately, this study may contribute to the development of atmospheric corrosion sensors based on electrochemical methods.

2. EXPERIMENTAL

Materials and reagents: Zinc (99.99%, wt%), 304 stainless steel (304SS), and 304 stainless steel tube (304SST, 2 mm inner diameter, 3 mm outer diameter) with a wall thickness of 0.5 mm were purchased from Tianjin Zhongpeng Metal Materials Co., Ltd., China. Chemicals, including NaCl (Sinopharm Chemical Reagent Co., Ltd.) and ethanol (Sinopharm Chemical Reagent Co., Ltd.), were used as received.

2.1. Experimental setup design

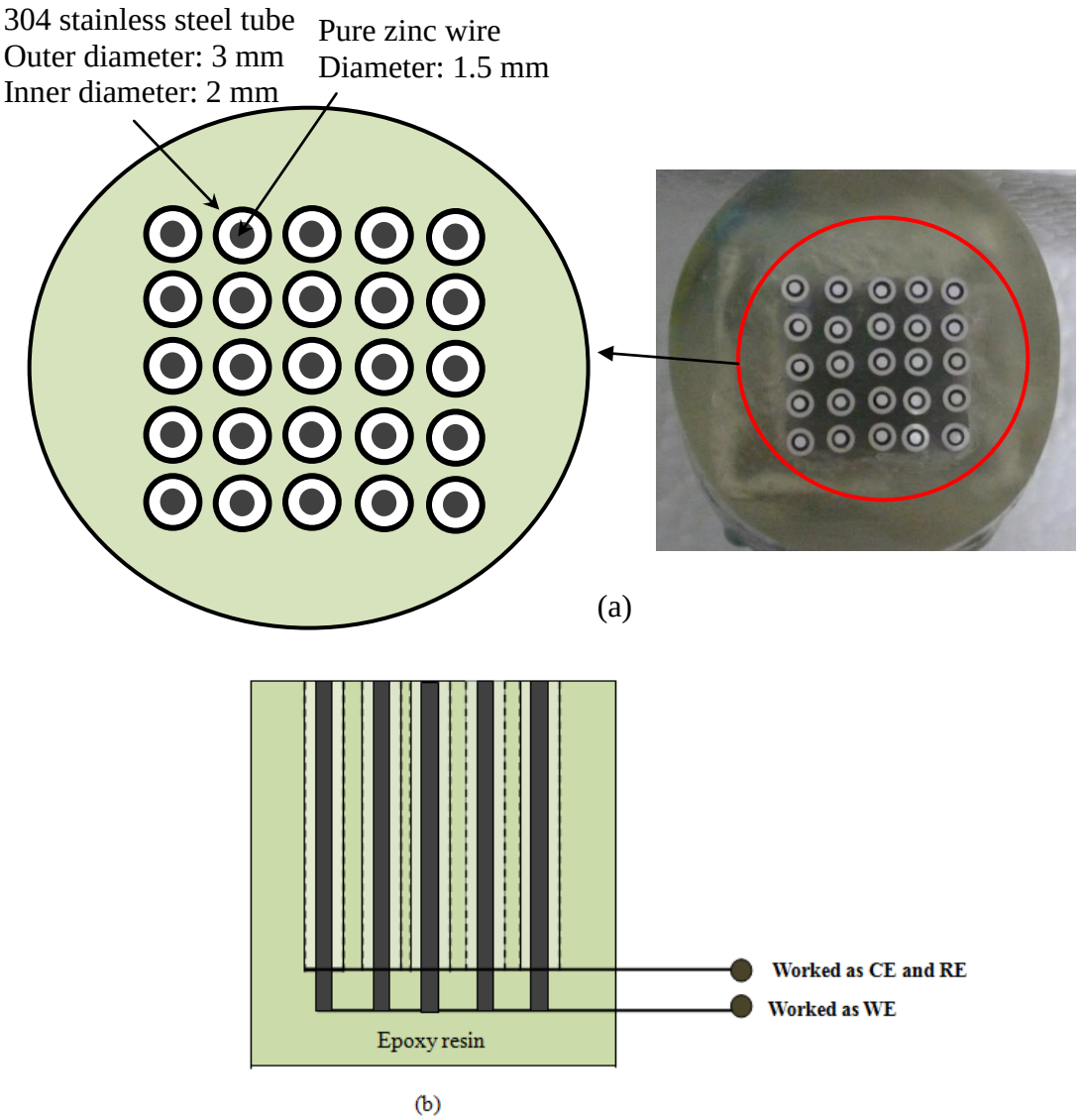

Figure 1. The design of the multielectrode sensors fabricated regularly arranged as a 5×5 matrix included 25 identical WEs which were made from pure zinc wires and 25 identical CEs made of 304SST. WE with 1.5 mm diameter was individually embedded into the centre of CE (2 mm inner diameter, 3 mm outer diameter) and separated from CE by a 0.15 mm thick thin insulator and an ambient-curing epoxy resin: (a) top view and (b) side view.

The experimental setup is illustrated in Fig. 1. The MSs used in this study included 25 identical WEs made from pure zinc wires and 25 identical CEs made of 304SSTs. The MSs were traditionally fabricated and arranged as a 5×5 matrix using a Bakelite mould. The WEs with 1.5 mm diameters were individually embedded into the centre of the CE and separated from the CE by a 0.15 mm thick thin insulator and an ambient-curing epoxy resin. All WEs and CEs were then embedded into the ambient curing epoxy resin. Prior to the electrochemical tests, the constructed MSs were gradually ground using a #1000 SiC paper, degreased with acetone for 2 min, and then dried under a cool air flow. Afterwards, the MS was placed in a desiccator for 24 h.

2.2. Environment simulation

The 40% to 100% RH range was maintained using a saturated salt solution. According to previous studies [16,36], NaCl particles remain in the original state at below 40% RH, and no corrosion products form on the sample surface. Thus, the 40% to 100% RH range was used in this study. To simulate the airborne NaCl particles found in the marine atmosphere, NaCl particles (200 μg cm^{-2}) were evenly deposited onto the MS surfaces. The deposition method was described in detail in a previous study [37]. The salinity in actual marine atmospheres can reach 150 μg cm^{-2} d^{-1} according to ISO 9223 [38]. The NaCl amount in this study was considered reasonable relative to the actual marine atmosphere. The MSs were then placed in different humidity chambers at constant temperature (25 °C). The airflow rate of the pure humid air passing through the exposure chamber was 100 mL min^{-1}.

2.3. Morphology of the electrode surface

To obtain clearer images, zinc samples (20 mm × 10 mm × 1 mm) and 304SS samples (20 mm × 10 mm × 1 mm) were gradually ground using a #3000 SiC paper, and then finely polished with a 2 μm diamond paste. Subsequently, all samples were rinsed with distilled water, degreased with acetone for 2 min, and dried under a cool air flow. NaCl particles (200 μg cm^{-2}) were evenly deposited onto the samples. Afterwards, the samples were placed in the atmospheric chamber. After the experiment, the morphologies of the corrosion products were analysed using SEM (KYKY-2800B, Beijing, China) at a field-emission energy of 10 keV.

2.4. Weight loss measurements

For the weight loss measurements, a large-area zinc (50 mm × 10 mm × 1 mm) sample was used, and the weight before and after corrosion was measured. The corrosion products were chemically removed by immersion in an NH_4Cl solution (100 g L^{-1}) at 70 ^{o}C according to ISO 8407 [39]. After complete removal of the corrosion products, the samples were washed with copious amounts of distilled water, dried, and then weighed to determine their weight loss. The measurements were made using a microbalance with a ±2 μg (±0.2 μg cm^{-2}) precision. The average weight loss of three repeat experiments was used in the calculation.

2.5. Electrochemical measurements

All electrochemical measurements were performed using a CHI660D electrochemical workstation (Shanghai Chenhua Device Company, China). EIS measurements were conducted with the frequencies from 100 kHz to 10 mHz at open circuit potential with a potential perturbation of ±5 mV. The EIS spectra of the electrodes with NaCl particles were recorded in situ in the test atmospheric chamber. Three repeated measurements were performed to determine the reproducibility.

3. RESULTS AND DISCUSSION.

3.1. Morphologies of corrosion products

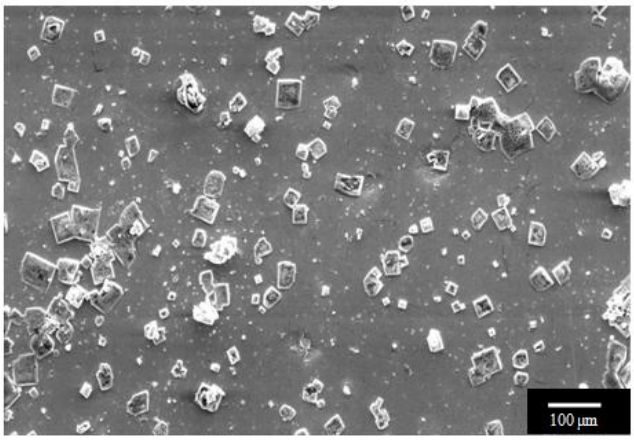

Figure 2. The morphology on the zinc sample covered by 200 µg cm^{-2} NaCl particles at 40% RH and 25 ^{o}C after 168 h of exposure.

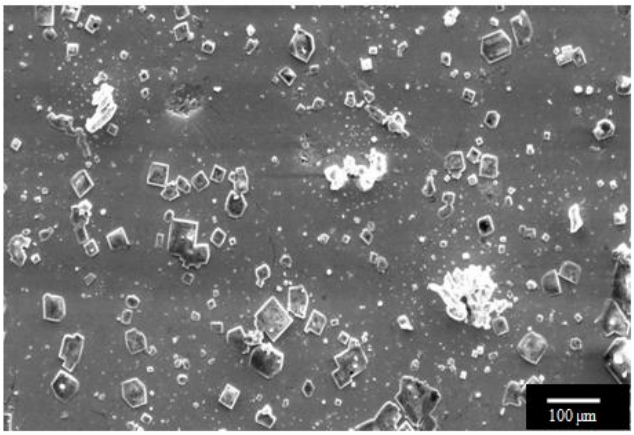

Figure 3. The morphology on the zinc sample covered by 200 µg cm^{-2} NaCl particles at 60% RH and 25 ^{o}C after 168 h of exposure.

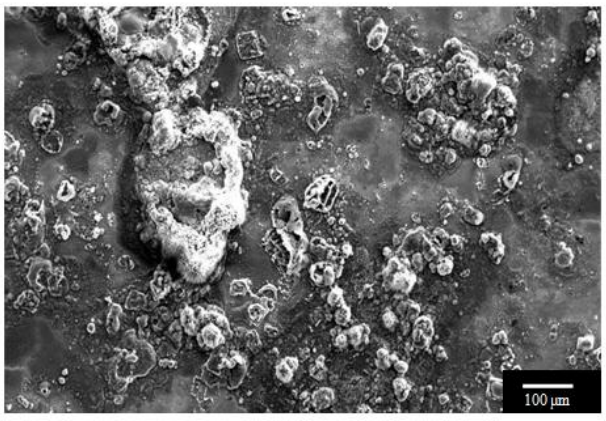

Figure 4. The morphology on the zinc sample covered by 200 µg cm^{-2} NaCl particles at 75% RH and 25 ^{o}C after 168 h of exposure.

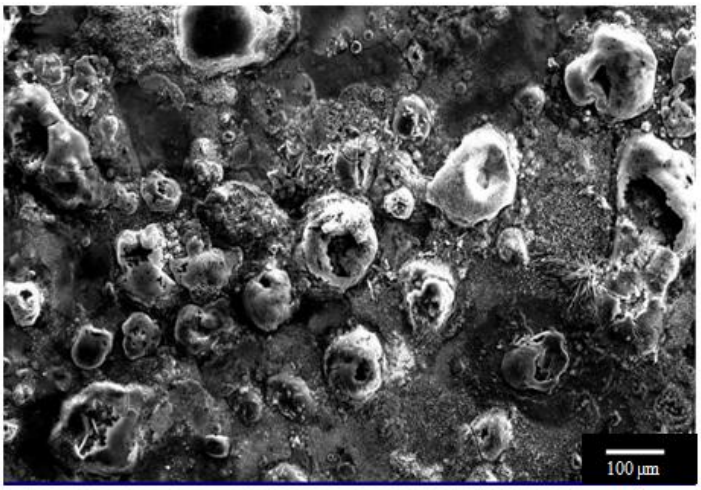

Figure 5. The morphology on the zinc sample covered by 200 μg cm^{-2} NaCl particles at 85% RH and 25 ^{o}C after 168 h of exposure.

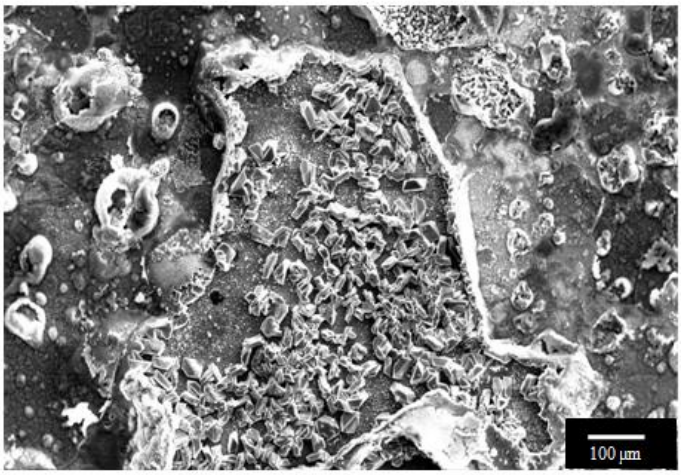

Figure 6. The morphology on the zinc sample covered by 200 μg cm^{-2} NaCl particles at 97% RH and 25 ^{o}C after 168 h of exposure.

The surface morphologies of zinc in the simulated marine environment are shown in Figs. 2-6.

Figs. 2 and 3 show that no corrosion products formed on the sample surface after 168 h of exposure under 40% and 60% RH. All NaCl particles remained in their original state as cubic particles. A similar behaviour was observed in a previous study [16]. The 40% and 60% RH were considerably below the NaCl deliquescence point (75% RH). Thus, no particles disappeared with increasing time. Fig. 4 shows that the NaCl particles dissolved in the moisture electrolyte layer, and that the corrosion products were sporadically dispersed on the electrode surface at 75% RH. At 85% RH, the sample appeared to undergo severe local corrosion and subsequently produced flower bud-shaped local corrosion products (Fig. 5) that eventually nearly covered the entire electrode surface. A similar effect was observed at 97% RH (Fig. 6); however, the corrosion on the electrode surface was more general compared with those that occurred at 75% and 85% RH.

As reported in a previous study [40], when NaCl particles are exposed to 75% RH or above, the predeposited NaCl particles transform into electrolyte droplets. Outside the droplet a thin electrolyte film forms, caused by secondary spreading from the original droplet. The driving force is oxygen reduction [41]. Under the present exposure conditions, the NaCl particles formed small droplets at 75% and 85% RH and caused secondary spreading over a relatively small area compared with that at 97% RH. Therefore, after 168 h of exposure, the corrosion products at 75% and 85% RH were unable to cover the entire electrode surface. At 97% RH, the corrosion effects became stronger because a larger amount of water was absorbed and larger electrolyte layers formed on the entire electrode surface.

3.2. EIS measurements

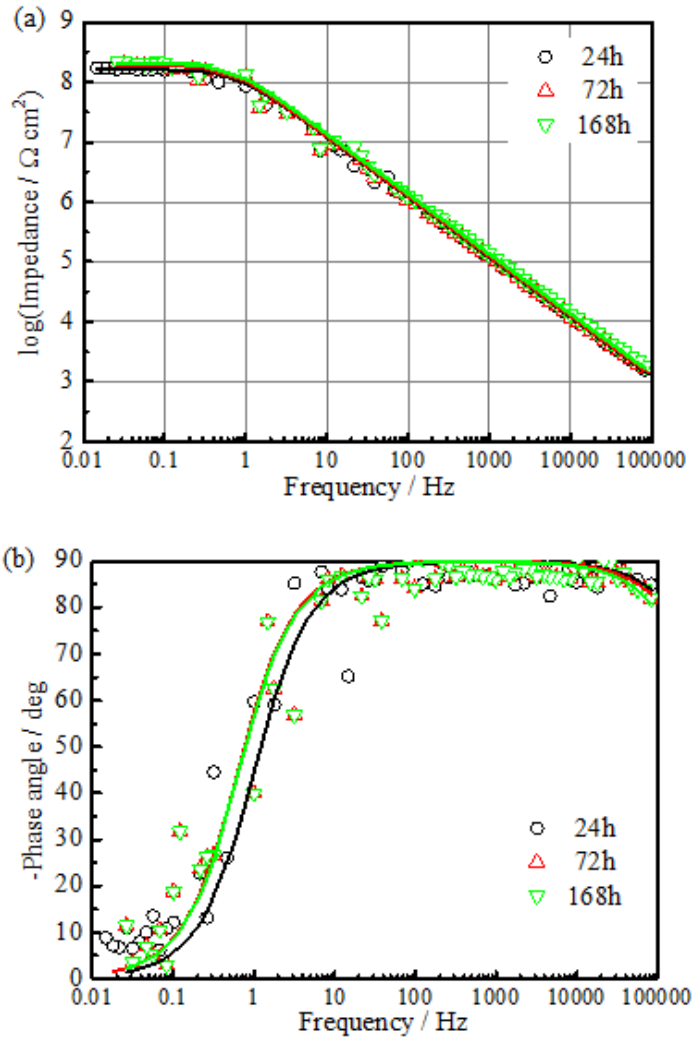

Figure 7. Experimental (dots with different symbols) and fitted (solid lines) impedance diagrams for the multielectrode sensors covered by 200 μg cm^{-2} NaCl particles at 40% RH and 25 ^{o}C during 168 h of exposure: (a) Bode magnitude plots and (b) Bode phase angle plots.

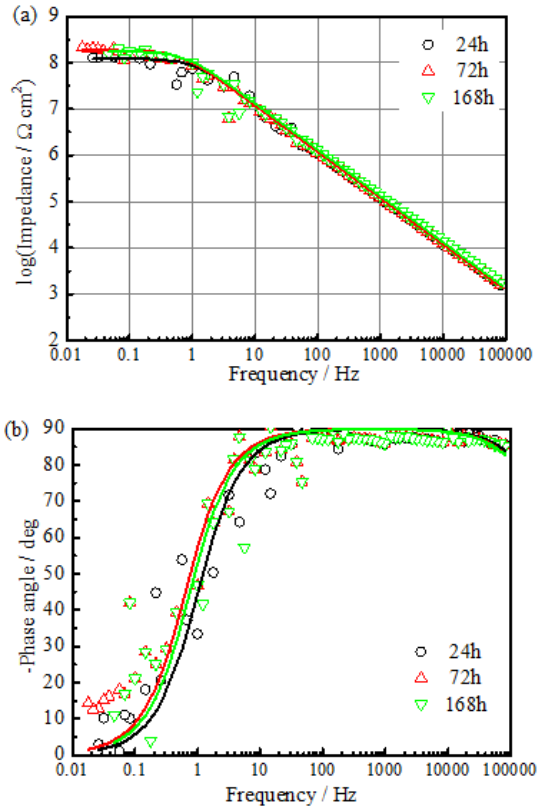

Figure 8. Experimental (dots with different symbols) and fitted (solid lines) impedance diagrams for the multielectrode sensors covered by 200 μg cm^{-2} NaCl particles at 60% RH and 25 ^{o}C during 168 h of exposure: (a) Bode magnitude plots and (b) Bode phase angle plots.

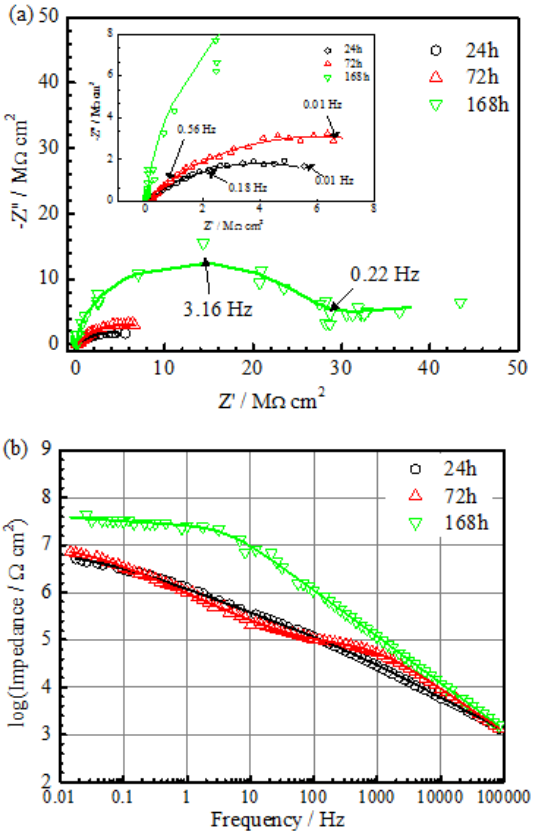

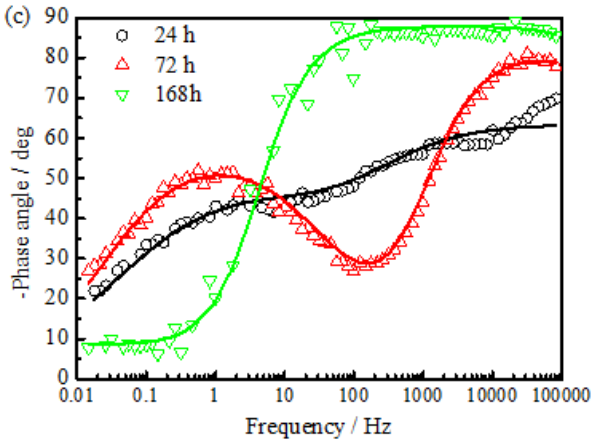

Figure 9. Experimental (dots with different symbols) and fitted (solid lines) impedance diagrams for the multielectrode sensors covered by 200 μg cm^{-2} NaCl particles at 75% RH and 25 ^{o}C during 168 h of exposure: (a) Nyquist plots, (b) Bode magnitude plots, and (c) Bode phase angle plots.

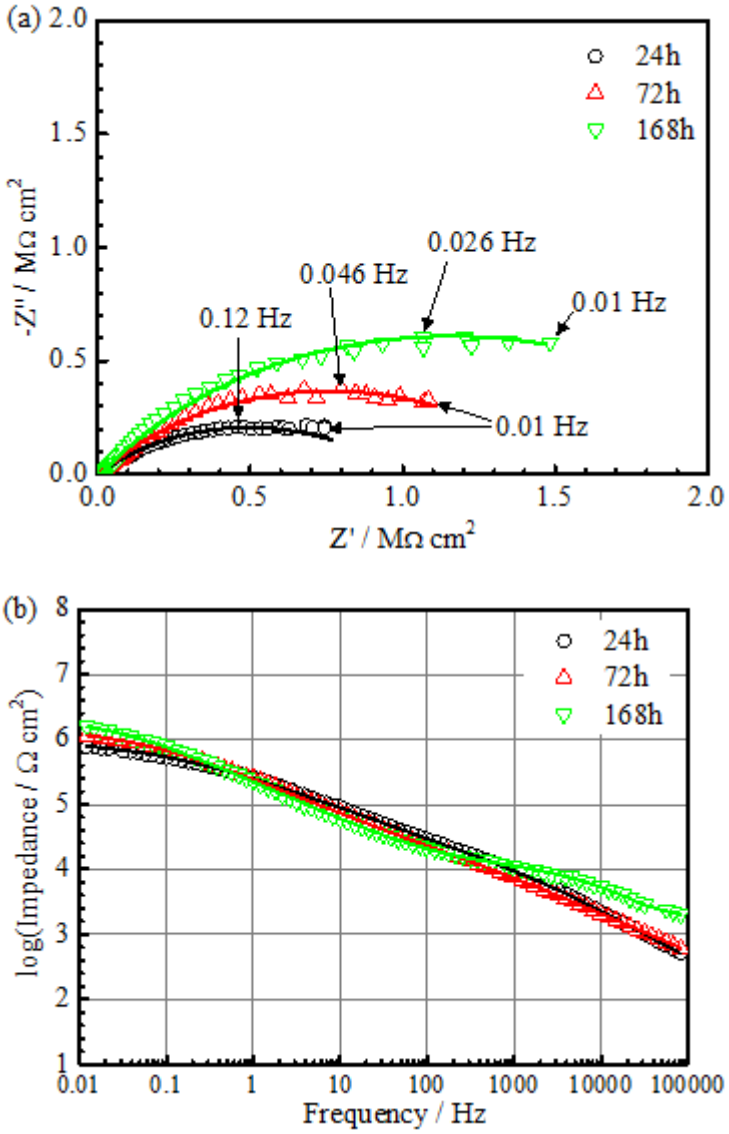

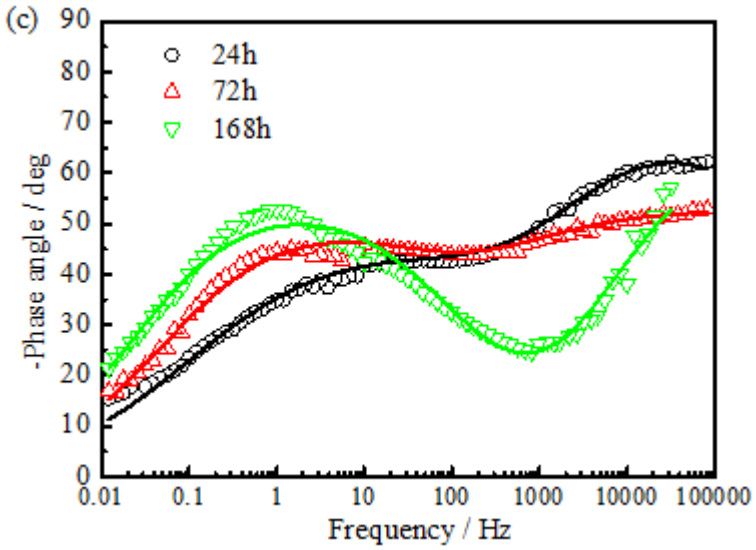

Figure 10. Experimental (dots with different symbols) and fitted (solid lines) impedance diagrams for the multielectrode sensors covered by 200 μg cm^{-2} NaCl particles at 85% RH and 25 ^{o}C during 168 h of exposure: (a) Nyquist plots, (b) Bode magnitude plots, and (c) Bode phase angle plots.

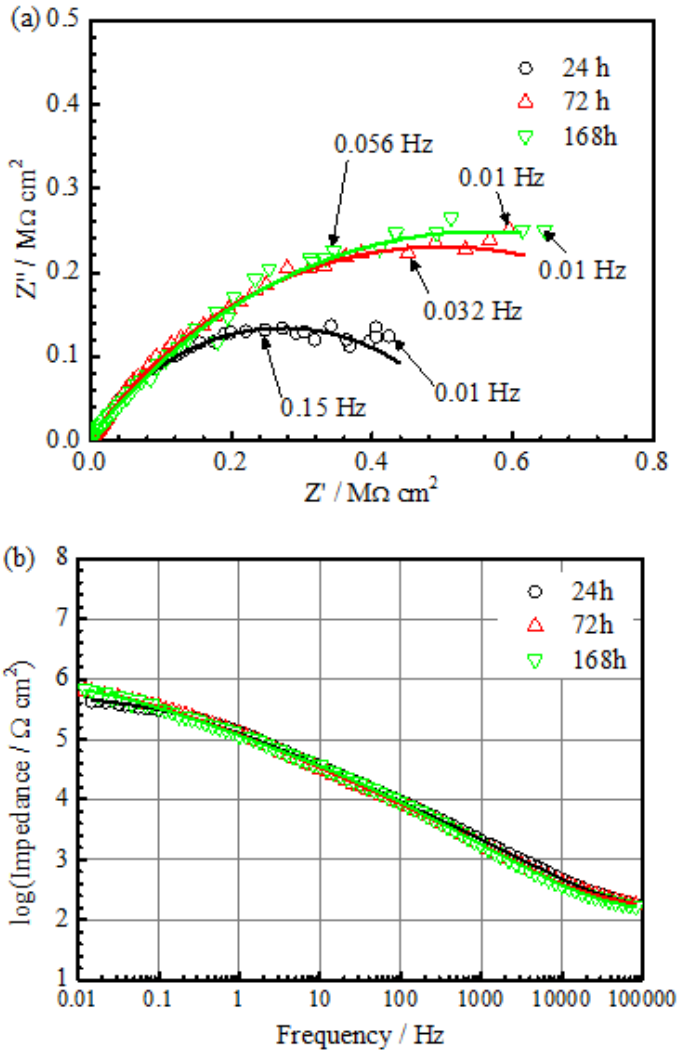

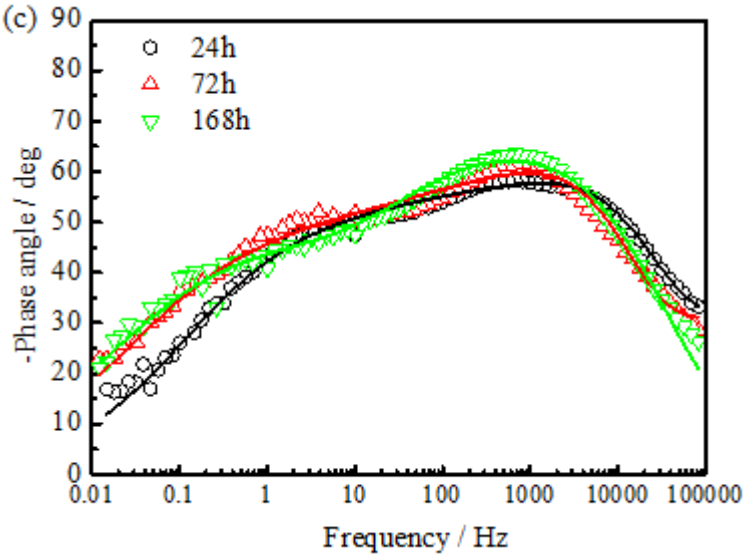

Figure 11. Experimental (dots with different symbols) and fitted (solid lines) impedance diagrams for the multielectrode sensors covered by 200 μg cm^{-2} NaCl particles at 97% RH and 25 ^{o}C during 168 h of exposure: (a) Nyquist plots, (b) Bode magnitude plots, and (c) Bode phase angle plots.

Three repeated measurements were performed to determine the reproducibility. However, only one representative measurement from the three experiments was selected. The EIS results for the MS under different RHs with different times are shown in Fig. 7 to 11. The measurements were conducted under 40% to 100% RH.

At 40% and 60% RH, Bode magnitude plots show one typical capacitance characteristic at HF with a slope coefficient equal to –1. Bode phase-angle plots show only one time constant (Figs. 7 and 8). Phipps et al. [36] reported that the amount of adsorbed water on a clean metal surface at 40% RH is less than two monolayers. However, the adsorbed water layer corresponds to three monolayers at 60% RH. Meanwhile, the moduli of impedance slightly increased with the exposure time at 40% and 60% RH; however, scattered EIS data were observed. Water adsorption on the electrode can provide the necessary electrolyte through which ions can migrate. The conductivity of the surface water film determines the dissolution rate of the anode as well as the migration rate of dissolved ions through the electrolyte, which in turn control the corrosion process. However, when adsorbed amount of water is less than three monolayers, the conductivity is significantly lower than that of a bulk electrolyte. Therefore, high ohmic drops at 40% and 60% RH control the corrosion process. Consequently, the moduli of impedance slightly increased with the exposure time at low RH.

The tests conducted at 40% and 60% RH yielded similar impedance results, and the moduli remained in the same order of magnitude (10^8 Ω cm^2) when the RH was increased from 40% to 60%. This phenomenon can be explained as follows: Yan et al. [42] reported that the resistance of two water monolayers is approximately 0.93×10^{10} Ω cm^2, whereas that of three water monolayers is approximately 1.15×10^{10} Ω cm^2. Therefore, the moduli (10^8 Ω cm^2) of impedance at 40% and 60% RH cannot be attributed to the resistance of absorbed water on the MS surface. In general, the impedance modulus at the HF region is responsible for the solution resistance. However, Fig. 2 and 3 show that the impedance modulus at the HF (10^5 Hz) region is 10^3 Ω cm^2, which is considerably lower than the

resistance of the adsorbed water layer. Therefore, the HF impedance modulus cannot be caused by the solution resistance. NaCl particles remained unchanged and no corrosion product formed on the electrode (Fig. 2 and 3) because the amount of absorbed water is insufficient to dissolve the particles at RH lower than the deliquescence point of the deposited particles. Moreover, the difference between resistances of the adsorbed water layers at 40% and 60% RH was minor. The 40% and 60% RH tests had different effects on the total impedance modulus; however, these effects were negligible. In conclusion, the EIS results in the 40% to 60% RH range reflect the electrode characteristics but not the corrosion on the Zn surface, as indicated by the similar impedance results and essentially unchanged modulus obtained at 40% and 60% RH.

The Bode diagrams for 75%, 85%, and 97% RH are shown in Fig. 9 to 11. The HF and LF domains generally exhibit two time constants. Most of the phase angles exceeded –45°. According to Nishikata *et al.* [12], a model for the current distribution can be estimated from the Bode plots. If the phase angles did not exceed –45°, the current distribution was considered uneven. However, if the phase angles exceeded –45°, the current distribution on the sample surface was considered uniform at least in the LF region when the frequency scan ranged from HF to LF. Therefore, the current was distributed uniformly on the MS surface and the uneven current distribution was not negligible for the entire stage. The EIS results reflect the integral corrosion behaviour of MSs. The MSs design integrates the applied current and thus enhances the electric signal detection. Therefore, errors resulting from uneven current distribution during electrochemical measurements are minimised by the proposed MSs.

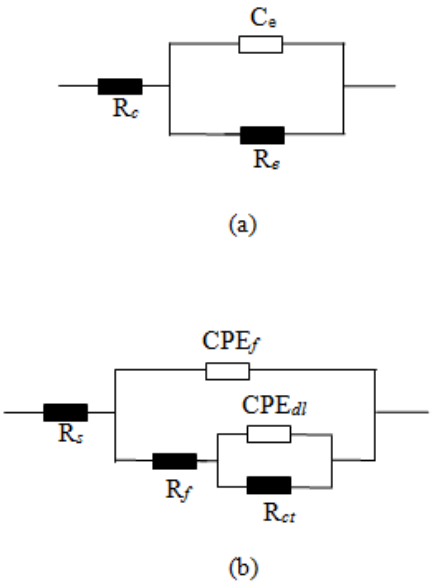

Figure 12. Equivalent circuits used for fitting the EIS data of the multielectrode sensors covered by 200 μg cm^{-2} NaCl particles with different RHs at 25 ^{o}C during 168 h of exposure. (a) Equivalent circuit at 40% and 60% RH, R_c is the contact resistance, C_e is the capacitance of epoxy resin, R_e is the resistance of epoxy resin. (b) Equivalent circuit at 75%, 85%, and 97% RH, R_s represents the solution resistance, R_{ct} is the charge-transfer resistance, CPE_{dl} is the double-layer capacitance at the surface of the electrolyte solution and zinc substrate, CPE_f and R_f are the capacitance and resistance of the insoluble corrosion products formed during exposure, respectively.

The surface morphologies of the zinc samples were used to verify the information shown in the EIS spectra. EIS reflects the signals on the WE.When an electrochemical reaction occurs on the electrode surface, the electrochemical process can be indicated by the electric double-layer capacitance and the charge-transfer resistance at the LF region. The EIS spectra obtained at 75% RH or above are assumed to reflect the corrosion process accurately. Thus, the EIS parameters can be appropriately used to evaluate the corrosion rate.

Table 1. Fitted parameters of EIS measurements of the multielectrode sensors covered by 200 μg cm^{-2} NaCl particles with 40% and 60% RH at 25 ^{o}C during 168 h of exposure.

RH (%)	*t* (h)	R_c (Ω cm^2)	C_e (nFcm^{-2})	R_e (MΩ cm^2)
40	24	222.1±31.6	1.5±0.3	175.2±11.4
	72	270±34.4	1.4±0.2	184.6±4.8
	168	306.6±81.1	1.4±0.2	200.5±5.1
60	24	161.1±38.6	1.3±0.1	122.6±2.8
	72	183.2±15.7	1.5±0.2	167.8±14.2
	168	225.6±19.2	1.3±0.1	174.6±5.6

Table 2. Fitted parameters of EIS measurements of the multielectrode sensors covered by 200 μg cm^{-2} NaCl particles with 75%, 85%, and 97% RH at 25 ^{o}C during 168 h of exposure.

RH (%)	*t* (h)	R_s (Ω cm^2)	CPE_f (nF cm^{-2} Hz^{1-n_f})	n_f	R_f (MΩ cm^2)	CPE_{dl} (μF cm^{-2} $Hz^{1-n_{dl}}$)	n_{dl}	R_{ct} (MΩ cm^2)
75	24	106.0±19.7	79.1±11.0	0.70	0.27±0.21	0.47±0.31	0.50	4.84±2.83
	72	83.4±16.4	7.3±2.8	0.92	0.16±0.12	0.67±0.35	0.64	9.63±1.01
	168	83.5±21.5	4.8±3.2	0.98	17.37±6.57	0.33±0.25	0.37	27.28±12.75
85	24	60.2±5.8	109.2±13.6	0.76	0.03±0.02	2.3±1.5	0.49	0.69±0.26
	72	17.6±7.2	767.0±207.8	0.59	0.02±0.02	4.5±2.2	0.57	1.08±0.34
	168	40.4±2.9	54.6±11.2	0.71	0.02±0.01	3.5±3.4	0.62	1.98±0.33
97	24	35.2±9.3	2719±547.7	0.57	(6.3±2.8)×10^{-4}	0.07±0.03	0.86	0.42±0.11
	72	10.4±8.8	2992±369.2	0.54	(2.5±1.3)×10^{-4}	0.1±0.05	0.87	0.73±0.24
	168	140.1±56.1	676.6±121.2	0.75	0.03±0.02	2.4±0.5	0.50	0.82±0.24

The corrosion characteristics were further verified by analysing the measured impedance based on the equivalent circuits (Fig. 12). Fig. 12a is used to fit EIS spectra at 40% and 60% RH; Fig. 12b is used to fit EIS spectra at 75%, 85%, and 97% RH. The data was fitted using ZSimpWin software. R_c is the contact resistance, C_e is the capacitance of epoxy resin, R_e is the resistance of epoxy resin, R_s represents the solution resistance, R_{ct} is the charge-transfer resistance, CPE_{dl} is the double-layer capacitance at the surface of the electrolyte solution and zinc substrate. CPE_f and R_f are the capacitance and resistance of the insoluble corrosion products formed during exposure, respectively, whereas

CPE_{dl} and CPE_f are the constant phase angle elements used in place of a capacitor to compensate for the non-homogeneity in the system. The impedance of CPE_{dl} and CPE_f is equal to $(Y_0(jw)^n)^{-1}$, where w is the AC-voltage angular frequency (rad s^{-1}), and Y_0 and n are the frequency-independent parameters. As shown in Fig.7 to 11, the two given equivalent circuits fit the experimental results well for nearly the entire frequency range. This result indicates the suitability of the given equivalent circuits for interpreting the corrosion behaviour of MS in the simulated marine atmospheric environment. Table 1 shows that C_e and R_e exhibited negligible changes with increasing exposure time at 40% and 60% RH. These findings further confirm that the EIS results reflect the electrode characteristics.

Table 2 shows the parameters obtained from the fitted EIS results at 75%, 85%, and 97% RH. The EIS spectra show no characteristic features of diffusion, such as a straight line in the LF region, which is related to the diffusion of electroactive species in the electrolyte layer. This result indicates that the electrochemical reactions were controlled by a Faradic process. Therefore, the reciprocal of the charge-transfer resistance ($1/R_{ct}$) from MS can be used to monitor instantaneous atmospheric corrosion under 75% to 97% RH in actual field environments [16, 43]. The variation in the mean $1/R_{ct}$ from three repeated measurements is shown in Fig. 13.

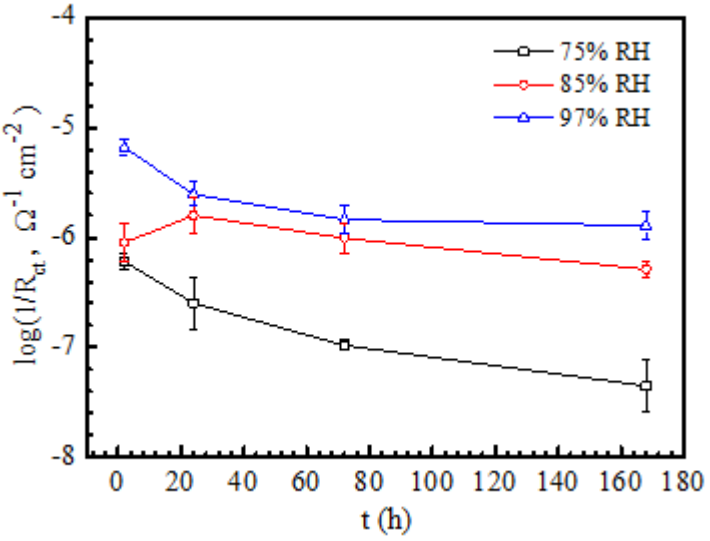

Figure 13. The time dependence of $1/R_{ct}$ of monitoring electrode in the 75% to 97% RH range during 168 h of exposure; the values of R_{ct} were obtained from the fitting EIS data based on Fig. 12b.

Generally, the polarisation resistance (R_p), which is obtained by subtracting the HF impedance from the LF impedance ($R_p = |Z(j\omega)|_{\omega\to 0} - |Z(j\omega)|_{\omega\to\infty}$), is inversely proportional to the corrosion rate [44], i.e. the higher the polarization resistance the better the corrosion resistance. Therefore, R_p was also used by Nishikata et al. [45] to evaluate the corrosion rate in an actual atmospheric environment. A previous study [34] showed that for zinc under a TEL, a proportional relationship continues to exist between the corrosion rate and the reciprocal of the polarisation resistance ($1/R_p$) even though the surface is covered with a thick corrosion product. Accordingly, $1/R_p$ was used as an index of the corrosion rate. A 10 mHz frequency may be too high for the measurement

of the actual polarisation resistance. However, the use of extremely LF is not suitable for atmospheric corrosion monitoring because impedance measurements at lower frequencies require longer time and the corrosion rate rapidly changes during atmospheric corrosion. The variation in the mean $1/R_p$ from three repeated measurements (Fig. 14) shows that $1/R_p$ exhibits a change trend similar to that shown in Fig. 13.

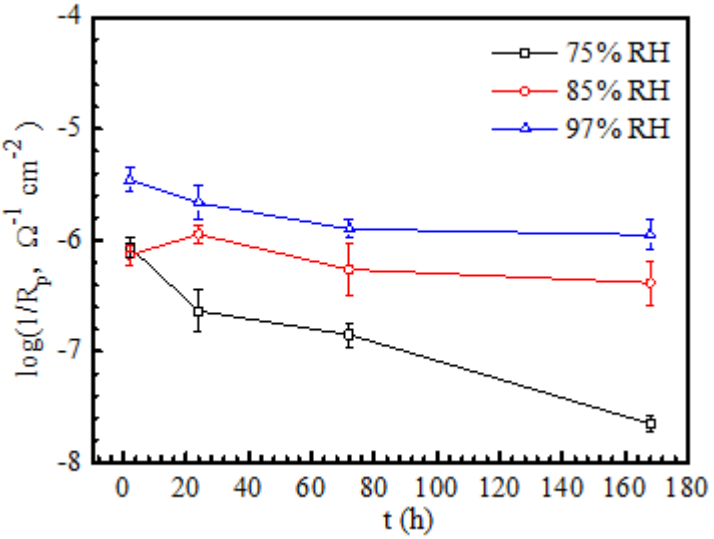

Figure 14. The time dependence of $1/R_p$ of monitoring electrode in the 75% to 97% RH range during 168 h of exposure; the values of R_p were obtained by subtracting a HF impedance from a LF impedance.

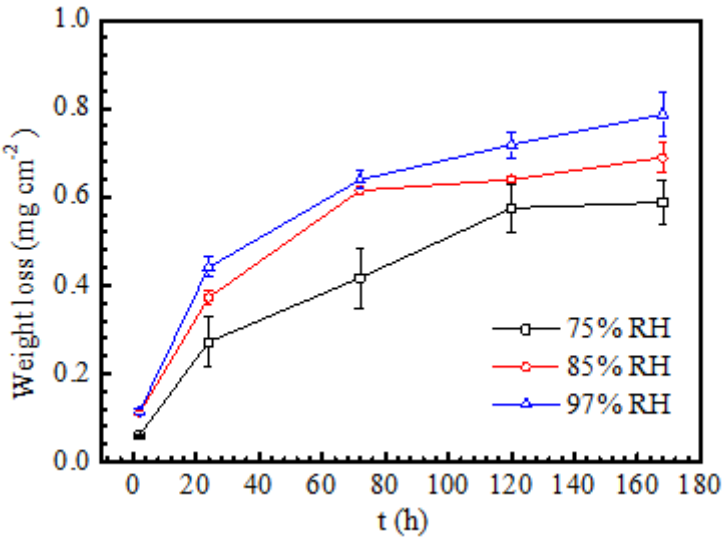

Figure 15. The time dependence of weight loss of zinc samples covered by 200 μg cm^{-2} NaCl particles at 25 ^{o}C in the 75% to 97% RH range during 168 h of exposure.

Weight loss tests were conducted to validate the feasibility of the EIS results further. Fig. 15 shows that the weight loss values increase with increasing RH. However, the slopes of the curves in

Fig. 15 decrease with the exposure time at the same RH. This finding indicates that the corrosion rate decreases with time and is consistent with the results shown in Figs. 16 and 17.

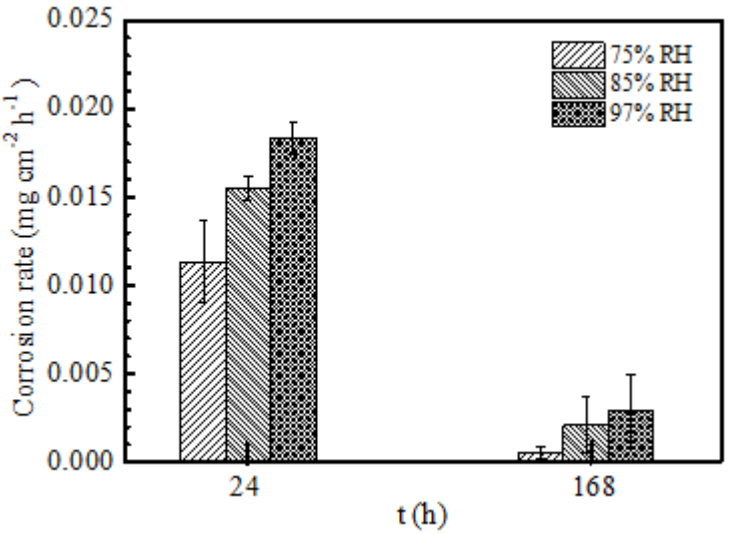

Figure 16. The average corrosion rate from the weight loss of zinc samples covered by 200 μg cm^{-2} NaCl particles in the first 24 h and in the last 24 h from Fig. 15.

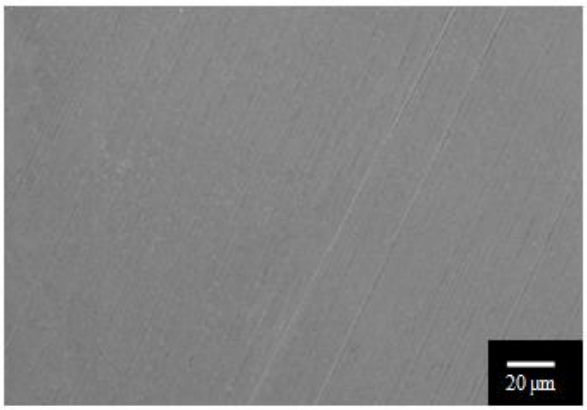

(a)

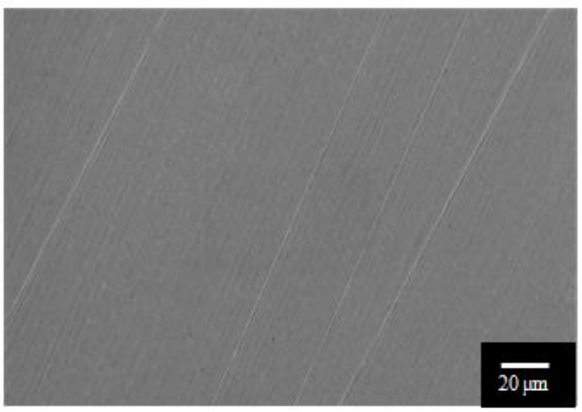

(b)

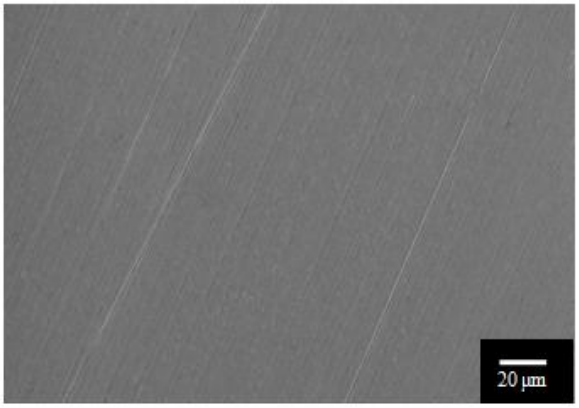

(c)

Figure 17. SEM micrographs of the 304SS surfaces covered by 200 μg cm^{-2} NaCl particles which were exposure to different RHs with immersion for 168 h (a) at 75% RH, (b) at 85% RH, and (c) at 97% RH after washing off the NaCl particles in distilled water.

To evaluate the reliability of $1/R_{ct}$ and $1/R_p$ with weight loss, the average corrosion rate was obtained from the weight loss results. Fig. 16 shows that average corrosion rates in the first 24 h and the last 24 h can be ranked as 97% RH > 85% RH > 75% RH. EIS clearly yielded results that are consistent with the average corrosion rates calculated from the weight loss measurements. Therefore, the data obtained from EIS analyses are valid. The model for the EIS spectra was subsequently used at 75% to 100% RH to determine the atmospheric corrosion rate.

3.3. The suitability of the CE

In a two-electrode system, the WE and the CE impedances are in series, and the system impedance is the sum of the WE and CE impedances. Although the impedance of the CE contributes to the system impedance, the change of the system impedance is only related to the WE impedance if the CE impedance does not change with time. To verify the stability of the CE impedance in MS, 200 μg cm^{-2} NaCl particles were evenly deposited onto the 304SS surfaces. Then the samples were placed in the 75%, 85%, and 97% RH chambers, respectively. After the experiment, the morphologies of the 304SS were analysed using SEM. As shown in Fig. 17, the 304SS surfaces have no sign of corrosion after washing off NaCl particles in distilled water. Tsutsumi et. al [46] have reported that the pitting corrosion of 304SS progressed only when the concentration of Cl^- exceeded 6 mol L^{-1}. A RH of 75% corresponds to a saturated sodium chloride solution (6 mol L^{-1}), 85% RH corresponds to 3.6 mol L^{-1} NaCl, and 97% RH corresponds to 0.8 mol L^{-1} NaCl [47]. Thus, the Cl^- concentration on the 304SS surfaces did not exceed 6 mol L^{-1} in present study, so the 304SS surfaces did not suffer from any corrosion. The CE impedance can be considered to be stable in MS during exposure of 168 h. Meanwhile, the results of weight loss tests (Fig. 15) also verified the feasibility of the EIS results in MSs. Based on above results, the CE used in MS was reliable.

4. CONCLUSIONS

The MSs based on the EIS technique, has been shown to be effective for studying simulated marine atmospheric corrosion behaviour in the environment seriously polluted with chloride ions in the 40% to 100% RH range. The main conclusions can be drawn as following:

1. In the 40% to 100% RH range, EIS spectra can be correctly used to evaluate the atmospheric corrosion process.

2. $1/R_{ct}$ obtained from the EIS spectra was successfully applied to monitor atmospheric corrosion rate. And $1/R_{ct}$ decreased with exposure time as well as $1/R_p$. Weight loss results further verified the applicability of the EIS spectra for evaluating the atmospheric corrosion rate.

3. Newly developed MSs are potentially useful for in situ monitoring the marine atmospheric corrosion.

ACKNOWLEDGEMENTS
The authors wish to acknowledge the financial supports of the National Department Public Benefit Research Foundation (201005028), Development Program of Science and Technology of Qingdao (12-4-4-yx) and National Basic Research Program of China（2014CB643304）.

References

1. A. Neufeld, I. Cole, A. Bond and S. Furman, *Corros. Sci.*, 44 (2002) 555.
2. N. Azmat, K. Ralston, B. Muddle and I. Cole, *Corros. Sci.*, 53 (2011) 1604.
3. X. Liao, F. Cao, L. Zheng, W. Liu, A. Chen, J. Zhang and C. Cao, *Corros. Sci.*, 53 (2011) 3289.
4. Y. Su and R. Shemenski, *Surf. Interface Anal.*, 40 (2008) 1183.
5. S. Hastuty, A. Nishikata and T. Tsuru, *Corros. Sci.*, 52 (2010) 2035.
6. J. Chen, J. Wang, E. Han and W. Ke, *Corros. Sci.*, 49 (2007) 1625.
7. T. Tran, C. Fiaud, E. Sutter and A. Villanova, *Corros. Sci.*, 45 (2003) 2787.
8. M. Wadsak, T. Aastrup, I. Wallinder, C. Leygraf and M. Schreiner, *Corros. Sci.*, 44 (2002) 791.
9. Y. Chen, H. Zeng, L. Wei and H. Shih, *Mater. Sci. Eng., A*, 398 (2005) 47.
10. M. Natesan, G. Venkatachari and N. Palaniswamy, *Corros. Sci.*, 48 (2006) 3584.
11. W. Jia and T. Tsuru, *J. Chin. Soc. Corros. Prot.*, 15 (1995) 180.
12. A. Nishikata, Y. Ichihara and T. Tsuru, *Corros. Sci.*, 37 (1995) 897.
13. G. El-Mahdy, A. Nishikata and T. Tsuru, *Corros. Sci.*, 42 (2000) 1509.
14. I. Shitanda, A. Okumura, M. Itagaki, K. Watanabe and Y. Asano, *Sens. Actuators B: Chem.*, 139 (2009) 292.
15. Y. Tan, *Sens. Actuators B: Chem.*, 139 (2009) 688.
16. C. Li, Y. Ma, Y. Li and F. Wang, *Corros. Sci.*, 52 (2010) 3677.
17. E. Schindelholz, R. Kelly, I. Cole, W. Ganther and T. Muster, *Corros. Sci.*, 67 (2013) 233.
18. G. Gallo and J. Popovics, *Corros. Sci.*, 63 (2012) 1.
19. C. Thee, L. Hao, J. Dong, X. Mu, X. Wei, X. Li and W. Ke, *Corros. Sci.*, 78 (2014) 130.
20. L. Nyrkova, S. Polyakov, S. Osadchuk, S. Mel'nychuk and N. Hapula, *Mater. Sci.*, 47 (2012) 683.
21. M. Stratmann and H. Streckel, *Corros. Sci.*, 30 (1990) 697.
22. M. Stratmann and H. Streckel, *Corros. Sci.*, 30 (1990) 681.
23. T. Zhang, C. Chen, Y. Shao, G. Meng, F. Wang, X. Li and C. Dong, *Electrochim. Acta*, 53 (2008) 7921.
24. S. Li, Y. Kim, S. Jung, H. Song and S. Lee, *Sens. Actuators B: Chem.*, 120 (2007) 368.
25. V. Zivica, *Constr. Build. Mater.*, 14 (2000) 351.

26. L. Yang, R. Pabalan, L. Browning and D. Dunn, in: R. J. Finch, D.B. Bullen (Eds.), Scientific Basis for Nuclear Waste Management XXVI, M.R.S. Symposium Proceedings, *Mater. Res. Soc. Warrendale, PA:*, 757 (2003) 791.
27. L. Yang, R. Pabalan and D. Dunn, *The 204th Meeting of the Electrochemical Society*, Abstract 465, Extended Abstract Volume 2003-II.
28. L. Yang, R.. Pabalan, L. Browning and G. Cragnolino, in: *Proceedings of the NACE International*, Houston, Texas, 2003, Paper No. 03426.
29. F. Mansfeld and J. V. Kenkel, *Corros. Sci.*, 16 (1976) 111.
30. F. Mansfeld, *J. Electrochem. Soc.*, 135 (1988) 1354.
31. E. Dubuisson, P. Lavie, F. Dalard, J. Caire and S. Szunerits, *Corros. Sci*., 49 (2007) 910.
32. A. Yadav, F. Suzuki, A. Nishikata and T. Tsuru, *Electrochim. Acta*, 49 (2004) 2725.
33. Y. J. Tan, *Corrosion*, 50 (1994) 266.
34. Y. J. Tan, *Corrosion*, 54 (1998) 403.
35. Y. Tan, N. Aung and T. Liu, *Corros. Sci.*, 48 (2006) 23.
36. P. Phipps and D. Rice, *ACS Symp. Ser*., 89 (1979) 235.
37. Z. Chen, S. Zakipour, D. Persson and C. Leygraf, *Corrosion*, 60 (2004) 479.
38. ISO 9223, *Classication, ISO, Geneva*, 1992.
39. ISO 8407, *ISO, Switzerland*, 2009(E).
40. Z. Chen, D. Persson and C. Leygraf, *Corros. Sci.*, 50 (2008) 111.
41. C. Chen, C. Breslin and F. Mansfeld, *Mater. Corros.*, 49 (1998) 569.
42. B. Yan, S. L. Meilink,G. Warren and P. Wynblatt, *IEEE Transactions on*, 10 (1987) 247.
43. H. Huang, Z. Dong, Z. Chen and X. Guo, *Corros. Sci.*, 53 (2011) 1230.
44. A. Nishikata, Y. Ichihara, Y. Hayashi and T. Tsuru, *J. Electrochem. Soc.*, 144 (1997) 1244.
45. A. Nishikata, F. Suzuki and T. Tsuru, *Corros. Sci.*, 47 (2005) 2578.
46. Y. Tsutsumi, A. Nishikata and T. Tsuru, *Corros. Sci.*, 49 (2007) 1394.
47. Z. Chen and R. Kelly, *J. Electrochem. Soc.*, 157 (2010) 69.